VEGF and the Fab fragment of a humanized neutralizing antibody: crystal structure of the complex at 2.4 Å resolution and mutational analysis of the interface

Yves A Muller[1,2], Yvonne Chen[1], Hans W Christinger[1], Bing Li[1], Brian C Cunningham[1], Henry B Lowman[1] and Abraham M de Vos[1]*

Background: Vascular endothelial growth factor (VEGF) is a highly specific angiogenic growth factor; anti-angiogenic treatment through inhibition of receptor activation by VEGF might have important therapeutic applications in diseases such as diabetic retinopathy and cancer. A neutralizing anti-VEGF antibody shown to suppress tumor growth in an *in vivo* murine model has been used as the basis for production of a humanized version.

Results: We present the crystal structure of the complex between VEGF and the Fab fragment of this humanized antibody, as well as a comprehensive alanine-scanning analysis of the contact residues on both sides of the interface. Although the VEGF residues critical for antibody binding are distinct from those important for high-affinity receptor binding, they occupy a common region on VEGF, demonstrating that the neutralizing effect of antibody binding results from steric blocking of VEGF–receptor interactions. Of the residues buried in the VEGF–Fab interface, only a small number are critical for high-affinity binding; the essential VEGF residues interact with those of the Fab fragment, generating a remarkable functional complementarity at the interface.

Conclusions: Our findings suggest that the character of antigen–antibody interfaces is similar to that of other protein–protein interfaces, such as ligand–receptor interactions; in the case of VEGF, the principal difference is that the residues essential for binding to the Fab fragment are concentrated in one continuous segment of polypeptide chain, whereas those essential for binding to the receptor are distributed over four different segments and span across the dimer interface.

Addresses: [1]Department of Protein Engineering, Genentech, Inc., 1 DNA Way, South San Francisco, CA 94080, USA and [2]Forschungsgruppe Kristallographie, Max-Delbrück-Centrum für Molekulare Medizin, Robert-Rössle-Strasse 10, D-13122 Berlin-Buch, Germany.

*Corresponding author.
E-mail: devos@gene.com

Introduction

Vascular endothelial growth factor (VEGF) is a highly specific angiogenic factor that has been implicated both in the *de novo* formation of blood vessels during embryogenesis (vasculogensis) and in the sprouting of new blood vessels from pre-existing ones (angiogenesis) [1–3]. The importance of VEGF in normal blood vessel development is emphasized by the observation that deletion of a single VEGF allele is lethal [4,5]. Furthermore, excessive and pathogenic angiogenesis plays a crucial role in a number of diseases, such as diabetic retinopathy and cancer [3]. The high specificity of VEGF for proliferation of vascular endothelial cells makes VEGF antagonists prime candidates for the suppression of pathogenic angiogenesis. This assumption has been substantiated by the suppression of tumor growth *in vivo* following treatment with anti-VEGF antibodies in a murine model [6]. These results prompted the engineering of a humanized version of murine neutralizing anti-VEGF antibody A4.6.1 [7,8], in order to investigate the beneficial effects of anti-angiogenic treatment in humans.

There are two known cellular receptors of VEGF, KDR (kinase domain receptor), which triggers the angiogenic response, and Fms-like tyrosine kinase 1 (Flt-1), the function of which is, as yet, poorly understood [9]. The same 115 N-terminal residues of VEGF are shared by a number of different splicing isoforms that range from 121 to 206 residues in length [10]. Plasmin cleavage of the longer forms shows that the receptor-binding functionality is contained within the first 110 residues [11]. The crystal structure of a truncated construct of VEGF (residues 8–109) [12] demonstrates that VEGF is a member of the cystine knot growth factor family (for a review, see [13]). Extensive mutagenesis data allowed for the mapping of the binding epitopes for KDR and Flt-1 onto the surface of VEGF [14,15] — the binding site was shown to be localized on the two symmetrical poles of the dimer [15]. This general location of the receptor-binding site was confirmed by the crystal structure of VEGF in complex with domain 2 of Flt-1 [16]. This structure also revealed that although the binding determinants for both receptors, as deduced from the mutagenesis studies, overlap

only partially, almost all these residues are in contact with domain 2 of Flt-1, suggesting that VEGF binds to KDR and Flt-1 in a similar fashion.

Neutralizing monoclonal antibody A4.6.1 binds tightly to VEGF, and this binding event prevents receptor activation [6]. In order to gain further insights into the mechanism of action of the antibody, we determined the crystal structure at 2.4 Å resolution of its humanized antigen-binding fragment, Fab-12 [8], in complex with the receptor-binding domain of VEGF. A comparison of this structure with those of free VEGF and of VEGF bound to domain 2 of Flt-1 shows that the neutralization mechanism of the antibody involves steric blocking of the receptor site, and not induced conformational changes in the ligand. We also performed an extensive alanine-scanning mutagenesis analysis [17] of both the combining site of the Fab fragment and the binding epitope of VEGF. Although alanine-scanning mutagenesis of the complementarity-determining regions (CDRs) in order to determine the relative contribution of individual residues to antigen binding has been reported before (for example, [18]), this is the first comprehensive mutational analysis of both the antibody and its antigen in combination with detailed structural information. The results show that only a small proportion of the residues in the interface are important for high-affinity binding, and the important residues of the antibody interact with those of the antigen to generate a remarkable 'functional' complementarity. These findings suggest that antigen–antibody interactions are qualitatively similar to other protein–protein interactions, such as those between receptors and their ligands [19].

Results

Accuracy of the crystallographic model

The crystal structure of the complex between the receptor-binding domain of VEGF (residues 8–109) [20] and the humanized Fab fragment, Fab-12 [8], of monoclonal antibody A4.6.1 was determined at 2.4 Å resolution and refined to a crystallographic R value of 19.6% (free R value 26.6%, Table 1). The crystallographic asymmetric unit contains two Fab molecules bound to the symmetrical poles of the VEGF dimer, and the molecular dyad of the VEGF dimer coincides with the noncrystallographic twofold symmetry of the complex (Figure 1). In both monomers of VEGF, only residues 14–107 are defined by their electron density. In both Fab molecules, the C-terminal residue Cys214 of the light (L) chain is missing and the six C-terminal residues Ser215–Thr220 are disordered in both heavy (H) chains. In addition, loop 128–133 in the constant domain of both heavy chains could not be placed with confidence and was therefore omitted from the model.

The coordinate error of the model as deduced from a σ_A plot [21] is ~0.35 Å; deviations from target-model geometry are 0.012 Å for bond lengths and 1.66° for bond angles.

Table 1

Crystallographic analysis.

Crystallization and data collection	
Space group	P2$_1$
Cell parameters a, b, c (Å)	89.86, 66.98, 140.51
β (°)	94.27
Resolution (Å)	20–2.4 (2.48–2.40)*
Unique reflections	63,147
Average redundancy	3.8
Average I / σ	8.6 (3.5)*
Overall completeness (%)	96.0 (81.3)*
R$_{merge}$† (%)	7.1 (12.8)*
Model	
Total no. of residues	1050
Contents of asymmetric unit	2 Fab fragments, 1 VEGF dimer
No. of solvent molecules	549
Total non-H atoms	8695
Average B factor (Å^2)	42.0
Diffraction agreement	
Resolution (Å)	8.0–2.4
R value (%)	19.6 (31.2)*
No. of reflections	54 493
Free R value (%)	26.6 (34.1)*
No. of reflections	5 908
Anisotropic correction, B$_{11}$, B$_{22}$, B$_{33}$, B$_{13}$ (Å^2)	3.7, −8.5, 4.8, −0.31
Stereochemistry	
Rmsd	
in bonds (Å)	0.012
in angles (°)	1.66
in temperature factors of bonded atoms (Å^2)	
overall	3.8
mainchain	2.6
sidechain	5.0

*Values for the highest resolution shell given in parenthesis. †R$_{merge}$ is defined as follows: R$_{merge}$ = 100 $\Sigma|I_1 - I_2|/\Sigma(I_1 + I_2)$

Of all 1050 residues, 89.4% are located in the most favorable regions [22] of the Ramachandran plot. Four residues are located in disallowed regions, namely residues Ser30$_{VL}$ and Thr51$_{VL}$ (V$_L$ denotes that the residues are located in the variable region of the light chain) of both Fab molecules in the asymmetric unit. They are part of the CDRs L1 and L2 and will be discussed below. As a result of the noncrystallographic symmetry restraints applied during refinement, the root mean square deviations (rmsds) between equivalent residues are small, namely 0.27 Å for the mainchain atoms (0.45 Å for all atoms) between the VEGF monomers, 0.17 Å (0.40 Å) for the V$_L$ domains, 0.42 Å (0.72 Å) for C$_L$ (light chain, constant, 0.16 Å (0.19 Å) for V$_H$ (heavy chain, variable), and 0.40 Å (0.60 Å) for the C$_{H1}$ (heavy chain, constant) domains.

The average temperature factor of the model is 40.5 Å^2. Although the average temperature factor of the VEGF dimer at 40.6 Å^2 is close to this, the average temperature factors of the two Fab fragments are 23.0 Å^2 and 61.4 Å^2, respectively (Figure 2). This difference is entirely accounted

for by the differences in mobility between the constant domains, because the variable domains have similar average temperature factors of 23.7 $Å^2$ and 28.4 $Å^2$, respectively. It is striking that the lowest temperature factors within both VEGF monomers are found for residues involved in the VEGF–Fab interface (Figure 2a); moreover, these temperature factors are very similar to the average observed for the variable domains. As these residues have higher than average temperature factors in 12 independent copies of free VEGF [12,15], Fab binding appears to have stabilized this region, enabling it to form a well-ordered intermolecular core that extends from VEGF to the variable domain of the Fab fragment.

The constant domain of one Fab fragment has a very high average temperature factor of 100 $Å^2$. This high thermal mobility is due to the almost complete lack of crystal-packing contacts for this domain; similar differences in mobility between the constant and variable parts of a Fab fragment have been observed before [23]. It should be noted that the presence of the second, crystallographically independent Fab fragment enabled us to model the average position of this domain with accuracy. This approach is not unlike the use of nuclear magnetic resonance (NMR) restraints to introduce additional information in the refinement of ribosomal protein L9 [24], which had similarly high thermal factors.

Overall structure of VEGF and anti-VEGF Fab

VEGF is a homodimeric protein and belongs to the family of cystine knot growth factors, members of which share a similar monomer fold, but differ in their dimerization mode [13]. The structure of the receptor-binding domain (residues 8–109) of VEGF consists of a central four-stranded β sheet that displays the characteristic cystine knot at one end [13] and possesses a small hydrophobic core at the other end [12,16]. This hydrophobic core is generated by residues from loop regions connecting the strands of the central β sheet, together with residues displayed on the N-terminal α helix of the second subunit, across the dimer interface. The dimerization mode of the VEGF homodimer is similar to that observed for platelet-derived growth factor [25] — a dyad axis oriented perpendicular to the β sheet places the two four-stranded β sheets side by side. No mainchain–mainchain hydrogen bonds are observed between strands across the interface, however.

The overall structure of VEGF in complex with the Fab fragment is very similar to the unbound structure previously reported [12]. The two monomers in the crystallographic asymmetric unit can be superimposed onto the eight monomers observed in the 1.9 Å crystal structure with average rmsds of 0.73 Å (mainchain atoms, residues 15–105). These deviations are of the same magnitude as those among the eight monomers of free VEGF. Nevertheless, although the overall structure is preserved in the complex,
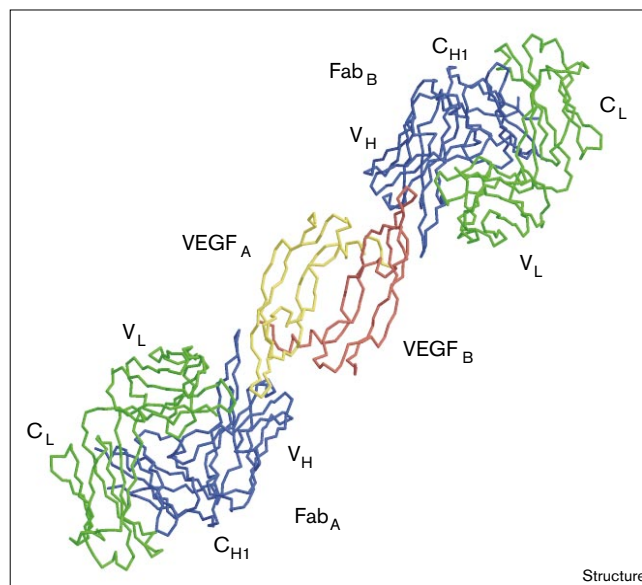
Cα representation of the complex of the VEGF dimer bound to two Fab molecules. The different chains are named as follows: VEGF$_A$ (yellow) and VEGF$_B$ (red), monomers A and B forming the VEGF dimer; Fab$_A$ and Fab$_B$, Fab molecules A and B; V$_L$, C$_L$, V$_H$, C$_{H1}$, variable domain and constant domain of the light chain (in green) and of the heavy chain (blue) of the Fab fragment, respectively.

small but significant differences are observed for some residues at the binding epitope of the antibody (see below).

The initial framework for the humanization of the anti-VEGF antibody was identical to that used for the anti-HER2 antibody, anti-p185[HER2] [26], but some adjustments in framework residues were required in order to obtain tight binding [7,8], resulting in an overall sequence identity of 88%. The structures of the variable domains of the anti-VEGF Fab can be superimposed on that of anti-p185[HER2] [27] with an rmsd of 1.04 Å (900 mainchain atoms used in the superposition); superimposing the constant domains yields a deviation of 0.59 Å (788 mainchain atoms). The two antibodies differ significantly in their elbow angle, despite having complete sequence identity among the residues in the interface between the variable and constant domains. For anti-p185[HER2], the elbow angle is about 160° (program CALC-AX; Joachim Meyer, personal communication), in comparison to 140° for both copies of the anti-VEGF Fab. Both these values fall within the range of 127°–225° previously reported for Fab fragments [28].

The CDR loops of the anti-VEGF Fab have the following canonical structures [29]: in the light chain, CDR L1 adopts canonical structure 2, L2 canonical structure 1, and L3 canonical structure 1; for the heavy chain, canonical structure 1 is observed for CDR H1, and canonical structure 2 for

Figure 2
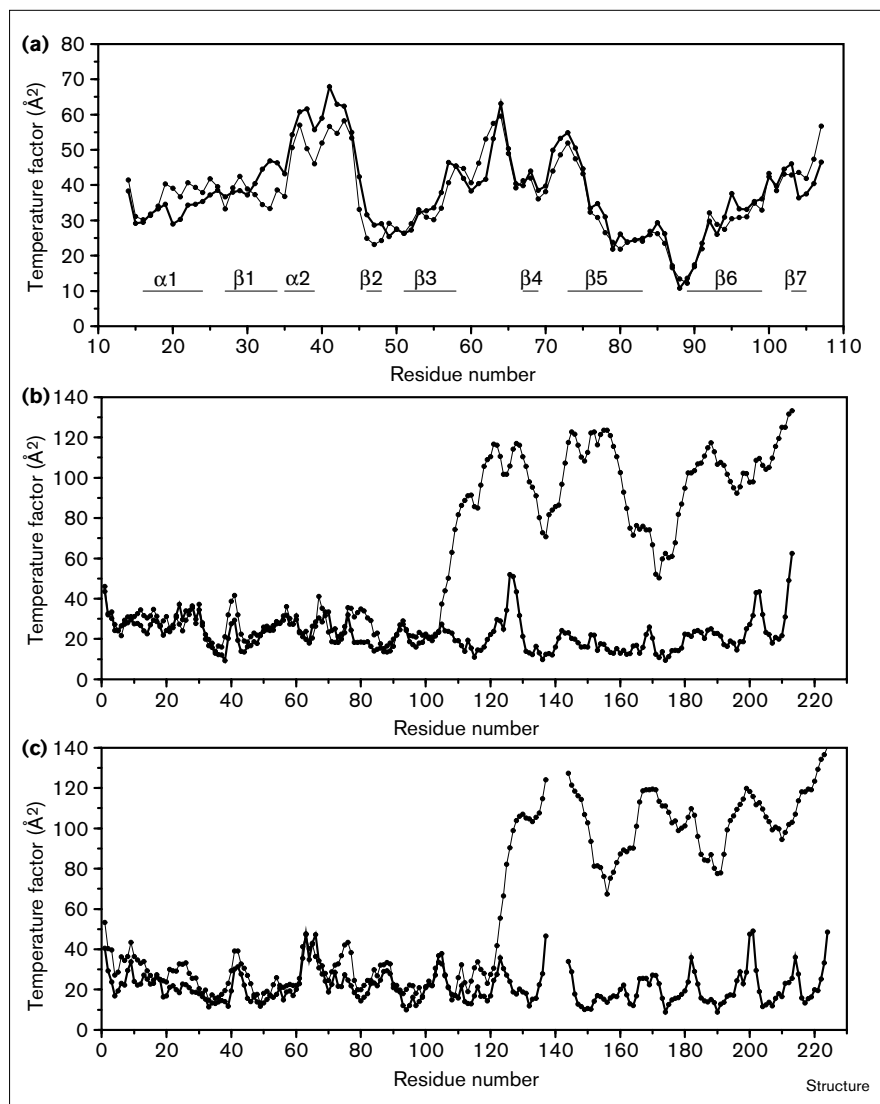
Average mainchain temperature factors per residue for the two copies of each molecule in the asymmetric unit (bold and thin lines). The temperature factors of **(a)** VEGF, **(b)** light chain and **(c)** heavy chain of the anti-VEGF Fab are shown. The lowest temperature factors in VEGF are observed for segment β5–β6, which binds to anti-VEGF. In this segment, the temperature factors are similar to the average temperature factors observed for the variable domains of anti-VEGF. Unusually high temperature factors are observed for the constant domains of the second anti-VEGF Fab molecule (see main text). Secondary structure elements of VEGF are defined as follows: α1 (residues 16–24), β1 (27–34), α2 (35–39), β2 (46–48), β3 (51–58), β4 (67–69), β5 (73–83), β6 (89–99) and β7 (103–105) [12].

H2. To date, only a single type of structure has been reported for CDR L2. In this CDR, the mainchain dihedral angles at Thr51 are close to those expected for left-handed α helices but nonetheless fall into disallowed regions [22] of the Ramachandran plot. Interestingly, the same observation has been made for other Fab fragments whose structures have been determined (e.g. see [27,30,31]). Thus, it appears that the angles observed at position 51 of CDR L2 constitute a real shift from a canonical left-handed helical conformation and that this reflects a general property of L2. A similar observation holds true for position 30 in canonical structure 2 of CDR L1.

Antigen–antibody interface

The anti-VEGF antibody binds VEGF at outer strands β5 and β6 (Figures 1 and 3), in close proximity to the β turn between these strands. The surface area buried in the antigen–antibody interface is 835 Å^2 for the antibody (Table 2) and 908 Å^2 for VEGF (Table 3). A total of 19 VEGF residues participate in the interface. Residues from strand β6 contribute 663 Å^2 (73% of the total buried surface area) and residues from strand β5 contribute 149 Å^2 (16%). The remaining contacts to the Fab fragment made by VEGF involve two residues displayed from the N-terminal helix α1 (43 Å^2, or 5%) and two residues from the loop connecting α2 to β2 (53 Å^2, or 6%; Figure 4).

Of the six CDRs of the antibody, L1 and L2 are not in contact with VEGF. In the remaining CDRs, a total of 25 residues participate in binding, resulting in the following buried surface areas: 68 Å^2 (8%) for L3, 125 Å^2 (15%) for H1, 222 Å^2 (27%) for H2, and 420 Å^2 (50%) for H3 (Table 2).

Figure 3

Schematic representation of the binding epitope of VEGF for the humanized anti-VEGF antibody. Residues buried in the interface as seen in the crystal structure are colored red; residues marked with yellow display a greater than 20-fold reduction in binding affinity when changed to alanine. For comparison, and to allow discussion of the neutralizing effect of the antibody, residues buried in the interface between VEGF and domain 2 of the Flt-1 receptor [16] are colored blue, and VEGF binding determinants for KDR [15] are in green. The position of the twofold axis of the VEGF dimer is indicated by a black ellipse.

Structure

The total buried surface area of 1744 Å² is typical of that observed for other Fab fragments bound to protein antigens [32,33]. The CDR usage conforms to the generalization that L2 is often not required for binding, while L3 and H3 are always involved [28,34]. Usually, CDRs of the heavy chain contribute a greater amount of buried surface than those of the light chain [32,34]. The ratio observed for the VEGF–Fab complex, however, with only 8% contributed by the light chain and 92% by the heavy chain, appears extreme.

The CDRs form a shallow cleft on the surface of the antibody. The walls of the cleft are formed by L3 and H3 on one side, and H1 and H2 on the opposite side. With the exception of His86, residues 86–94 of VEGF strand β6 are bound in an almost extended conformation along the floor of the cleft. His86 is at position i+2 of the type II β turn [35] that connects strand β5–β6. Adjacent to this histidine, a β bulge is formed between Gln87 and Gly88 of strand β6 and Lys84 of the adjacent strand, β5 (Figure 3). Residues 89–94 form a total of five main-chain–mainchain hydrogen bonds with the Fab fragment. Residues 89–91 are hydrogen bonded to residues 33–31 of CDR H1, forming a short antiparallel β ladder; a short parallel β ladder is formed between VEGF residues 91–93 and Tyr98–Gly100 of CDR H3. No mainchain–mainchain interactions with the Fab fragment are observed for residues 86–88.

Table 2

Alanine-scanning analysis of the Fab phage.

	V_L-residue number	IC_{50}(mutant)/ IC_{50}(wt)*	Buried area (Å^2)		V_H-residue number	IC_{50}(mutant)/ IC_{50}(wt)*	Buried area (Å^2)
L1	Arg24	1.3	0	H1	Gly26	2.3	0
	Ala25Ser	1.1	0		Tyr27	34 (44[†])	0
	Asn26	1.5	0		Thr28	1.3	0
	Glu27	1.2	0		Phe29	16	0
	Gln28	1.2	0		Thr30	1.3	4
	Leu29	1.4	0		Asn31	>150	86
	Ser30	1.5	0		Tyr32	>150	24
	Asn31	1.7	0		Gly33	6.1	11
	Tyr32	1.9	0		Met34	6.3	0
	Leu33	2.2	0		Asn35	66	0
	Asn34	3.7	0				
				H2	Trp50	>150	53
L2	Phe50	1.4	0		Ile51	3.8	0
	Thr51	0.78	0		Asn52	>150	35
	Ser52	0.75	0		Thr52A	8.6	2
	Ser53	0.76	0		Tyr53	8.7 (9.4[†])	96
	Leu54	0.86	0		Thr54	4.4	7
	His55	0.98	0		Gly55	1.1	0
	Ser56	0.85	0		Glu56	1.7	0
					Pro57	1.5	0
L3	Gln89	3.7	0		Thr58	2.6 (4.2[†])	29
	Gln90	2.7	0		Tyr59	2.0	0
	Tyr91	14	3		Ala60Ser	1.2	0
	Ser92	0.90	11		Ala61Ser	1.4	0
	Thr93	0.87	2		Asp62	1.4	0
	Val94	1.5	34		Phe63	0.97	0
	Pro95	3.5	0		Phe64	1.2	0
	Trp96	>150	18		Arg65	1.2	0
	Thr97	1.4	0				
				H3	Tyr95	150 (1800[†])	13
					Pro96	38	14
					His97	4.1	56
					Tyr98	3.8	122
					Tyr99	4.6	36
					Gly100	1.8	39
					Ser100A	0.7	3
					Ser100B	>150	42
					His100C	2.4 (3.8[†])	2
					Trp100D	>150	93
					Tyr100E	19	0
					Phe100F	25	0
					Asp101	1.9	0
					Val102A	1.3	0

*The IC_{50} measurements showed an average error of ~25%. [†]K_d(mutant)/K_d(wt) by BIAcore; wild type (Y0192) Fab shows an association rate of $4.1 \times 10^4 \text{ M}^{-1} \text{ s}^{-1}$ and a dissociation rate of $1.4 \times 10^{-4} \text{ M}^{-1} \text{ s}^{-1}$, yielding a K_d(wt) of 3.4 ± 0.9 nM.

The most prominent structural feature of the interface is the burial of Gly88 of VEGF in a deep pocket on the surface of the antibody-combining site (Figure 5). This pocket is best described as a four-walled box with each wall being made of the sidechain of a single aromatic residue, namely residues Trp96 of CDR L3, Trp50 of H2, and Tyr95 and Trp100D of H3. Gly88 of VEGF is sandwiched between the sidechains of Trp50 of CDR H2 and Trp100D of H3. As a result, its phi and psi angles are ~180°. In addition, hydrogen bonds are formed between Gln87 O of VEGF and Tyr95 Oη of CDR3 H3, as well as between Tyr95 Oη of H3 and Trp96 Nε1 of L3. A similar

molecular box contains Gly92 of VEGF, which is sandwiched between His97 and Tyr98 of CDR H3 and nearby residue, Tyr32 of CDR H1. Again, the mainchain torsion angles of Gly92 of VEGF are ~180°.

No salt bridges are found at the interface, but several sidechain-mediated polar interactions are present. The sidechain of Gln89 of VEGF is hydrogen bonded to Thr30 O and Thr52A NH of CDRs H1 and H2, respectively. The sidechain of His90 of VEGF is buried in a small pocket formed by Pro96, Tyr98, Ser100B and Trp100D of CDR H3. His90 Nε2 of VEGF is hydrogen

Table 3

Alanine-scanning analysis of VEGF.

VEGF residue	IC_{50}(mutant)/ IC_{50}(wt)*	Buried area ($\mathring{A}^2$)	Fab residues within 4.5 $\mathring{A}$[†]
Phe17	2.4	26	V_H: Asn31
Tyr21	2.5	17	V_H: Tyr53
Tyr45	4.5	29	V_H: Ser100B, Trp100D
Phe47	1	0	
Lys48	2.2	24	V_H: Tyr53
Gln79	5.6	13	V_H: His97
Ile80	2.6	1	V_H: Tyr98
Met81	74	36	V_H: Thr30, Asn31, Tyr53
Arg82	22	55	V_H: Tyr98, Gly100, Ser100A, Ser100B
Ile83	35	32	V_H: Asn52
Lys84	7.8	12	V_H: Trp100D
His86	2.3	74	V_L: Val94; VH: Trp50, Thr58
Gln87	1.4	115	V_L: Ser92, Val94, Trp96 V_H: Trp50, Tyr95, Trp100D
Gly88	40	37	V_H: Trp50, Tyr95, Trp100D
Gln89	102	131	V_H: Thr30, Asn31, Tyr32, Gly33, Trp50, Ile51, Asn52, Thr52A, Tyr53, Tyr95, Trp100D
His90	1.7	115	V_H: Asn31, Tyr32, Tyr95, Pro96, Tyr98, Ser100B, His100C, Trp100D
Ile91	3.5	75	V_H: Asn31, Tyr32, Pro96, His97, Tyr98
Gly92	107	32	V_H: His97, Tyr98
Glu93	4.9	79	V_H: His97, Tyr98, Tyr99, Gly100
Met94	5.0	5	V_H: Tyr98

*The IC_{50} measurements showed an average error of about 25%. All mutants with fivefold or more decreased affinity for mAb A4.6.1 bound within twofold of wild-type affinity to mAb 32.E.1 (data not shown), which has a separate, dimer-dependent binding epitope [15]. [†]Fab residues underlined are those with a more than 150-fold decrease in affinity to VEGF, when changed to alanine (see Table 2).

bonded to Ser100B Oγ of H3. In addition, Ser100B Oγ is hydrogen bonded to the guanidinium group of Arg82 of VEGF. The interface does not contain any ordered water molecules, although a number of waters mediating polar interactions between VEGF and the antibody are found at the periphery of the combining site. A sulfate ion was located in close proximity to the combining site. The sulfate is hydrogen bonded to Thr28, Asn31 and Tyr32 of CDR H1 of the Fab fragment, but there are no direct interactions with VEGF (an indirect interaction with the sidechain of Gln79 of VEGF is mediated by a water molecule). We believe that the presence of the sulfate is a crystallization artifact.

Alanine scanning of the interface

In order to assess the relative importance of the contact residues at the interface, a number of mutants, each with a

single residue changed to alanine, were generated for both VEGF and the Fab fragment. For the anti-VEGF Fab, the contributions of all 68 sidechains within the six CDRs were assessed by individual mutation of pY0192 Fab-phage (Figure 6) residues to alanine (or to serine for wild-type alanines). Relative binding affinities to VEGF were measured in competitive monovalent phage enzyme-linked immuno-absorbant assays (ELISAs) (see Materials and methods section). The IC_{50} (the concentration of competitor at which 50% inhibition of binding is observed) of the wild-type Fab phage for VEGF was measured at 4.7 ± 1.1 nM, comparing favorably to the measured K_d of 3.4 ± 0.9 nM for the purified wild-type Fab using BIAcore. The use of phage-ELISA techniques for measurement of binding affinities greatly facilitated the scanning of CDR residues. In order to assess the accuracy of this method, five alanine variants representing a wide range of apparent binding affinities by phage-ELISA were tested in a BIAcore assay in addition to the wild type. Within the uncertainties of each technique ($\pm 25\%$) excellent agreements are observed between both methods (Table 2), showing that the phage-ELISA technique can provide accurate measurements of relative binding affinities.

The alanine-scan phage variants displayed a range of affinities, from that of wild type to > 700 nM; all variants showed some VEGF-specific binding (Table 2). In particular, large decreases in affinity (> 150-fold, $-\Delta\Delta G > 3$ kcal/mol) resulted primarily from substitution of residues located within the heavy-chain CDRs: Asn31 and Tyr32 in H1; Trp50 and Asn52 in H2; and Tyr95, Ser100B, and Trp100D in H3. Among the light-chain CDR residues, only substitution of Trp96 produced so great an effect. Together, these positions define the primary functional sidechain-binding determinants. Less severe reductions in affinity (5–70-fold, $-\Delta\Delta G = 1$–2.5 kcal/mol) resulted from alanine substitutions at Tyr27, Phe29, Gly33, Met34, and Asn35 of H1, Thr52A and Tyr53 of H2, Pro96, Tyr99, Tyr100E, and Phe100F of H3, and at one light-chain position, Tyr91 of L3. Smaller, but significant, reductions in affinity (2–5-fold, $-\Delta\Delta G = 0.4$–1 kcal/mol) were also observed at many positions of the heavy-chain CDRs, including those at residues 26, 51, 54, 58–59, 97–98, 100C and 101, as well as at positions 32–34, 89–90, and 95 in the light-chain CDRs. The remaining CDR mutations, including those at the sites of expression-associated mutations Ser24Arg, Ser26Asn, Gln27Glu, Asp28Gln, and Ile29Leu in CDR L1 (see Materials and methods section), showed no significant effect upon VEGF binding affinity. Overall, the results suggest that a large energetic contribution to the Fab–VEGF interaction stems from a subset of CDR residues in H1, H2, and H3, with some contribution from L3.

The mutagenesis analysis of VEGF showed that 12 of the 19 alanine mutants tested displayed at least a fivefold decrease in binding to mAb (murine antibody) A4.6.1

Figure 4
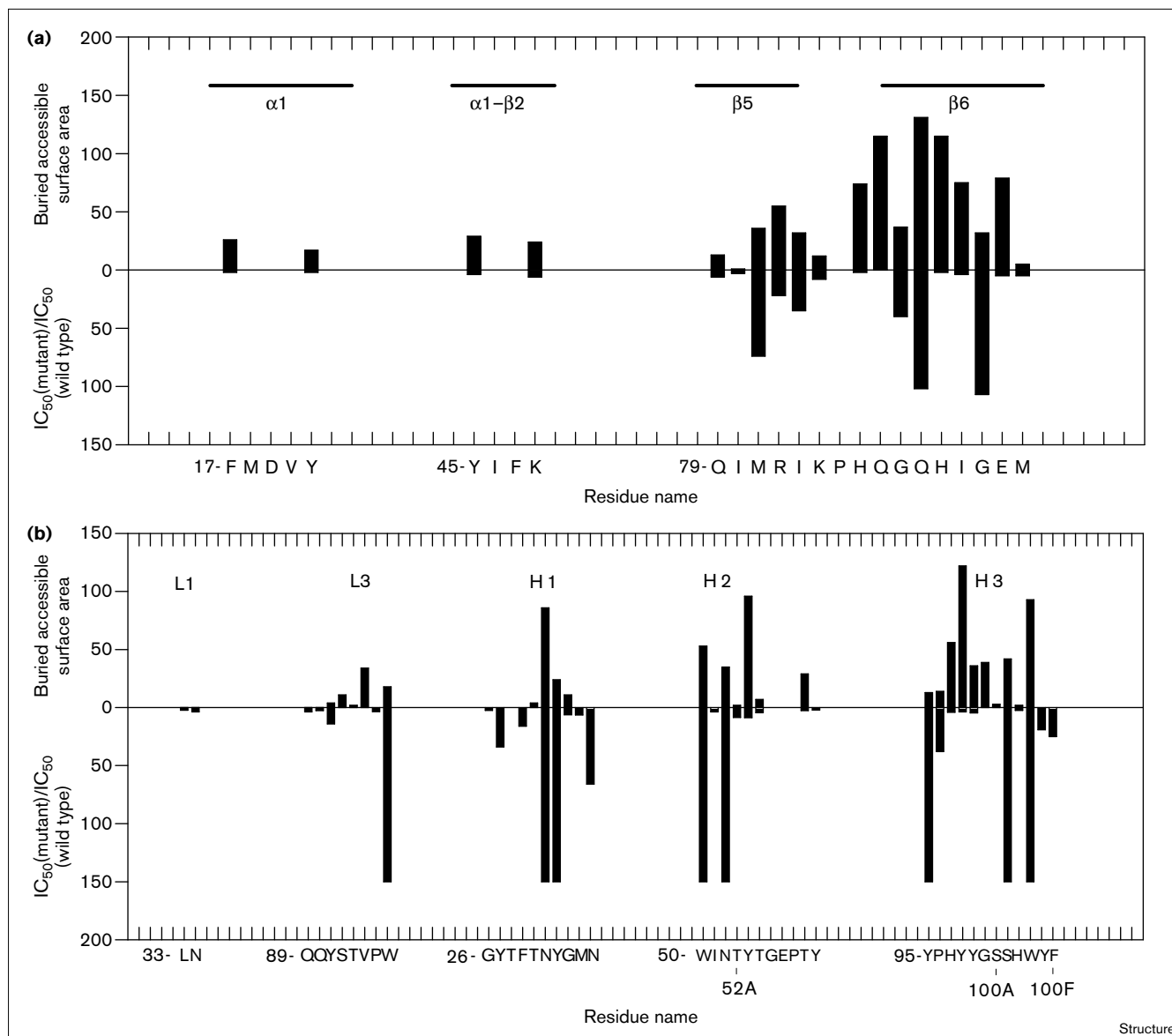
Comparison of accessible surface area buried in the VEGF–Fab interface and contributions of individual residues to the antibody binding as identified by alanine-scanning mutagenesis: **(a)** residues from VEGF, **(b)** residues from the anti-VEGF Fab.

(Table 3). Six of these mutants showed dominant effects, and reduced binding by factors of *22–107* fold (Table 3). These six residues are localized primarily within the 12-residue segment of VEGF that contains strands β5 and β6 along with the intervening β turn. Mutants of Met81, Arg82, Ile83, Gly88, Gln89, and Gly92 showed 74-, *22-*, 35-, 40-, 102- and 107-fold (−ΔΔG = 2–3 kcal/mol) decreases in affinity, respectively, relative to the wild type. Smaller, but significant, decreases in binding of about 5–8 fold (−ΔΔG = ~1 kcal/mol) were found for mutations at positions 48, 79, 84, 93 and 94. The overall structural integrity of the alanine mutants with a fivefold or greater effect on

mAb A4.6.1 binding was confirmed using a similar ELISA that measured binding affinity of the mutants to mAb 32.E.1, which has a separate, dimer-dependent, binding epitope [15].

Discussion
Antigen–antibody interface
A total of 25 residues of the Fab fragment become buried in the antigen–antibody interface upon binding to VEGF, together constituting the structural epitope. Eight of these residues are critical for binding, as defined by greater than 150-fold decreases in binding upon alanine substitution

Figure 5

Stereoviews of the interface between VEGF and the anti-VEGF Fab. For clarity, the only VEGF residues shown are those in segment β5–β6. **(a)** Surface of the antibody combining site and stick representation of segment β5–β6 of VEGF. The molecular surface of the light chain and heavy chain are shown in grey and blue, respectively. Residues of anti-VEGF critical for binding are shown in magenta. The termini and VEGF residues critical for binding are labeled. **(b)** Atomic detail of the antibody combining site using the same color coding as in (a). For simplicity, the mainchain of the anti-VEGF Fab is shown as a continuous ribbon. Illustrations drawn with the program GRASP [55].
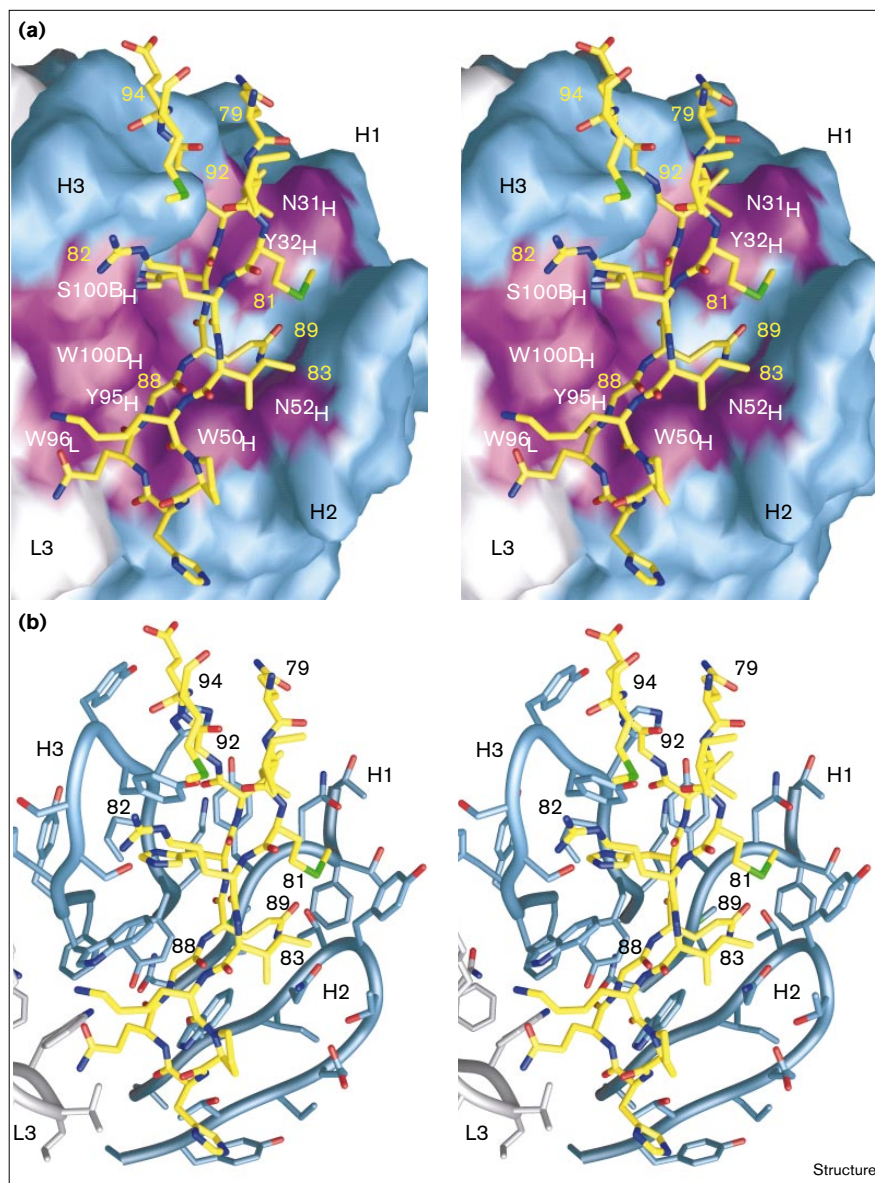
(Table 2), and form the functional epitope of the Fab fragment. Together, these eight residues contribute 360 Å^2 (44%) to the surface area buried in the interface. Five residues are aromatic, the remaining three being two asparagines and a serine. The high proportion of aromatic residues, in particular tyrosine and tryptophan, is a feature of the entire structural epitope, for which 11 residues are aromatic out of total number of 25. This bias has been noted before and reflects a general property of antibody combining sites [23,32,36].

On VEGF, the functional epitope is dominated by six residues; most important are Met81, Gln89 and Gly92, substitution of which reduces affinity by about 70–110 fold.

Slightly smaller, but still large, contributions (*22–40-fold* effects) are made by Arg82, Ile83, and Gly88. In general, alanine-scanning mutagenesis provides a useful method of assessing the relative contributions of individual side-chains to the binding energy [37]. Results at glycine positions are less meaningful, however, because substitution to alanine introduces a stiffening of the protein backbone and requires additional space to accommodate the additional Cβ atom, without providing information on the contribution of the wild-type residue to the free binding energy of the complex. In the case of the VEGF–Fab complex, the structure shows that steric hindrance is likely to be the cause of the decreased affinity of the glycine to alanine mutants at positions 88 and 92.

Figure 6

Sequence comparison of anti-VEGF Fab variants. Variant Fab-12 is a previously described humanized version of the murine antibody A4.6.1 [8]. Variant MB1.6 was isolated from an earlier Fab-phagemid library [7] and used to produce a Fab phagemid, called pY0101, similar to Fab-12. Variant Y0192, an expression-optimized derivative of Y0101 (see Materials and methods section for details), was used for the alanine-scanning mutagenesis described here. Residues are numbered sequentially (top) and according to Kabat *et al.* [56] (bottom). CDR regions are underlined. Residues unique to the respective sequences are indicated by shaded boxes.

The direct juxtaposition of important binding determinants from both functional epitopes is striking (Tables 2 and 3). The six dominant binding determinants of VEGF are in intimate contact with the Fab fragment (Figure 4a). The main structural feature is the binding of Gly88 of VEGF through the aromatic box formed by the sidechains of residues Trp96 of CDR L3, Trp50 of CDR H2, and Tyr95 and Trp100D of CDR H3 (Figure 5). In this case, considering the functional importance of both the glycine and the surrounding Fab residues, the direct interactions between the glycine and the box appear to provide significant binding energy. In contrast, for the aromatic box surrounding Gly92 of VEGF, none of the sidechains of the Fab residues is crucial for binding. The structure shows that in this case substitution with alanine is likely to interfere with the formation of the numerous mainchain–mainchain hydrogen bonds observed across the interface at this position. Thus, the steric requirements of this region are likely to be critical for maximum affinity. Additional juxtapositions of important binding determinants are Met81 of VEGF and Tyr53 of H2, Arg82 of VEGF and Ser100B of H3, and Ile83 of VEGF and Asn52 of H2. Although no simple favorable interaction is observed for Ile83 of VEGF, its sidechain is in close contact to a critical CDR H2 residue, Asn52. Finally, the sidechain of VEGF Gln89 is involved in a number of hydrogen bonds with mainchain atoms of CDRs H1 and H2.

From the data presented here, the functional VEGF epitope for Fab binding appears to be rather small. Similar

Figure 7

Stereo representation illustrating the conformational change in strand β6 induced by the antibody upon binding to VEGF. The geometrically averaged Cα backbone calculated from the eight monomers present in the triclinic crystal form of free VEGF is shown in red. At each Cα position, the smallest ellipsoid that fits all Cα atoms of the eight monomers is displayed (calculated with program GEM [57]). The backbone conformation of strands β5–β6 as observed in the VEGF–Fab complex is shown in green. Although for most of the residues involved in binding the observed backbone conformation represents one out of the ensemble of eight structures observed in free VEGF, significant deviations occur for His90 and Gly92, whose Cα positions differ by more than 7.9σ and 10.6σ, respectively, from the positions in the ensemble.
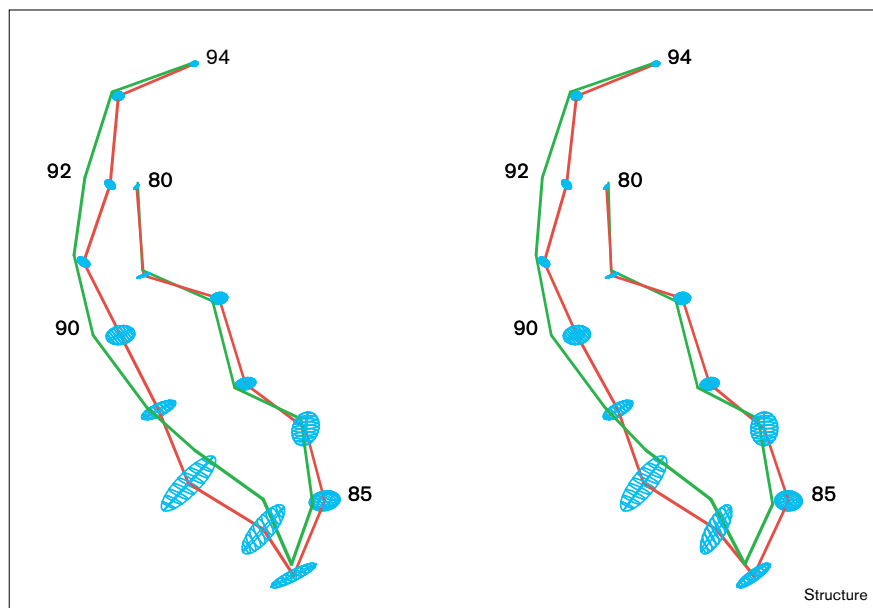
small binding epitopes have been deduced from theoretical considerations for the binding of lysozyme to two different antibodies, D1.3 and HyHEL-5 [38]. These calculations have been corroborated partially by competition studies with homologous avian lysozymes [39]. The size of the functional epitope identified for the anti-VEGF Fab fragment is similar to that identified for the humanized anti-p185[HER2] antibody [18], using the same method. In this case, however, both the functional epitope of the antigen and the crystal structure of the complex are missing. In the case of anti-p185[HER2], a set of only four important binding determinants were identified, namely His91$_{VL}$, Arg50$_{VH}$, Trp95$_{VH}$ and Tyr100A$_{VH}$ [18]. Here, too, aromatic residues prevail and the binding determinants cluster in a shallow pocket on the antibody surface.

General similarities exist between the VEGF–Fab interface and other protein–protein interactions. The interaction between human growth hormone and its receptor has been investigated using the same methods as described here, that is, structure determination of the complex [40,41] and exhaustive alanine-scanning mutagenesis of the binding partners [37,40,42]. In this case, of 32 hormone residues in contact with the receptor, only five contribute most of the binding energy; these are in contact with the five most important residues of the receptor, resulting in a remarkable degree of functional complementarity between the two epitopes [19]. From these studies, it was proposed that only a small subset of the residues buried in a protein–protein interface may be the principal contributor to the binding energy; in the growth hormone example, these residues are clustered

together in a small hydrophobic patch surrounded by polar interactions. A similar situation was observed in an analysis of the interaction between tissue factor and coagulation factor VIIa [43,44], where, again, only a small subset of residues contribute most to ligand affinity. In this case, however, these residues form several discontinuous clusters on the protein surface.

In most complexes between protein antigens and antibodies, a number of well-ordered water molecules are found within the combining site [45]. It has been proposed that water molecules are required in order to overcome imperfections in shape complementarity and that such imperfections are characteristic of protein–antibody interactions, possibly because, in contrast to other protein–protein interactions, antigen recognition has not been optimized through evolution, but rather depends on rapid selection pressure [33]. In the case of VEGF, no water molecules are buried in the antigen–Fab interface, and excellent complementarity is observed between segment β6 of VEGF and the combining site. Furthermore, the observation that in the complex the temperature factors of VEGF segment β5–β6 (Figure 2) are very similar to those of the variable domains of the antibody and considerably lower than the rest of VEGF suggests tight packing of the interface. It is worth noting that in the complex of VEGF with domain 2 of its Flt-1 receptor, a channel of water molecules is found in the interface [16]; similar water clusters have also been observed in the growth hormone–receptor interface [40]. Thus, water-mediated contacts are not specific to interfaces between antibody and antigenic protein. With respect to these findings, a remarkable similarity

is observed between the antibody–antigen recognition reported here and protein–protein interactions in general.

Conformational change upon binding

In addition to the crystal structure of the VEGF–Fab complex, the structure of unbound VEGF is also known [12,15]. The triclinic crystal structure contained eight independent copies of the molecule in the asymmetric unit, and superposition of the eight molecules made possible the identification of the conformationally flexible portions of the molecule. The highest deviations were observed within segment β5–β6, and it was shown that the eight conformations represent different 'snapshots' of a concerted 'up and down' loop movement [12]. In the Fab complex, this same segment is intimately involved in antibody binding. Superposition of this segment, as observed in the complex, onto the conformations seen in unbound VEGF shows that, overall, the bound conformation fits well within the range of conformational freedom observed in the unligated structure (Figure 7). Two of its Cα positions do not, however, fall within the range of conformational flexibility of the unbound state. The Cα of VEGF His90 is displaced by 1.3 Å; this corresponds to a 7.9σ movement when considering the standard deviation of the distance deviations among the eight monomers in unligated VEGF. Similarly, a 1.2 Å (10.6σ) displacement is observed for the Cα of VEGF Gly92 (Figure 7). We conclude that the anti-VEGF antibody selects one of the available multiple conformations of this loop upon binding, while inducing small but significant local changes at positions 90 and 92.

The neutralizing effect of anti-VEGF antibody

Binding of VEGF by the anti-VEGF antibody prevents the growth factor from binding to its receptors. The overall structure of residues 8–109 of unbound VEGF is identical to that in the complex with the Fab fragment, demonstrating that the neutralizing effect is not the result of antibody-induced conformational changes in the ligand preventing receptor binding. Recently, we determined the crystal structure of residues 8–109 of VEGF in complex with domain 2 of Flt-1 [16]. A comparison of both structures clearly explains the neutralizing effect of the antibody — of the 19 VEGF residues contributing to the interface in the VEGF–Fab complex, nine are also buried in the interface with domain 2 of Flt-1. It is worth noting that, of these, only a single residue, namely Ile83, is an important binding determinant for both the antibody and the receptor (Figure 3). The neutralizing effect therefore appears to be due to steric hindrance, and not due to competition for the same critical binding determinants.

Biological implications

A comparison of the structure of the VEGF–Fab complex with other antigen–antibody complex structures reveals that the binding mode of VEGF resembles that of linear peptides more closely than that of protein antigens. Whereas peptides are predominantly bound within deep grooves, protein antigens tend to interact at the periphery of the CDRs via a relatively flat surface [46]. Peptides bind predominantly in an almost extended conformation, usually with a β turn next to the terminus [28]. In VEGF, this motif corresponds to strand β6 together with the preceding type II β turn formed by residues Lys84–Gln87. A somewhat similar situation was observed in the recent crystal structure of the N-terminal domain of the interferon-γ receptor α chain in complex with Fab-A6 [23]. Here, too, most of the interactions of the Fab fragment (80%) are with a single continuous loop segment of the receptor, and additional segments make less extensive contributions, generating a discontinuous binding epitope.

Jones and Thornton [33] have shown that interfaces in nonpermanent and nonobligatory complexes, such as antigen–antibody and hormone–receptor interfaces; have smaller interaction surfaces, lower packing densities and involve more polar interactions than seen in permanent complexes that do not exist as independent entities, such as dimeric molecules. Our results on the VEGF–antibody and VEGF–receptor complexes are in agreement with this analysis. The principal difference we observe is the significant extent of fragmentation of the structural binding epitope in the latter, with fewer segments being involved for antigen–antibody interfaces [33]. This difference is even more pronounced when looking at the functional epitope, instead of the structural epitope. In VEGF the important residues all cluster within the continuous segment β5–β6; similar localization of binding determinants is observed for a second neutralizing antibody whose functional epitope resides primarily on helix α1 [15]. In contrast, the binding determinants of VEGF for kinase domain receptor (KDR) are distributed over four different segments [15].

Materials and methods

Complex formation and crystallization

Residues 8–109 of VEGF were expressed, refolded, and purified as previously described [20]. Purified Fab-12 fragment was obtained from Pat McKay (Process Sciences, Genentech, Inc.), mixed with VEGF in a 2.1:1 molar ratio, and purified by size exclusion chromatography (S-200, Pharmacia) in 30 mM Tris-HCl, pH 7.5, 0.4 M sodium chloride. The composition of the resulting complex was verified by SDS PAGE and size exclusion chromatography (data not shown). The protein solution was concentrated to $A_{280} = 7.8$, and used in crystallization trials. Initial hanging-drop experiments using the vapor-diffusion method resulted in isomorphous crystals from two different conditions (15% PEG, 10% isopropanol, 0.2 M ammonium sulfate, 0.1 M MES, pH 6.0; and 2 M ammonium sulfate, 2% MPD, 0.1 M bis-tris-propane, pH 6.5). Crystals used in the structure determination were grown from large sitting drops by equilibrating a mixture of 20 µl protein solution and 20 µl reservoir solution (15% PEG, 10% isopropanol, 0.2 M ammonium sulfate, 0.1 M MES, pH 6.0) against 30 ml reservoir solution. Monoclinic crystals grew to a size of 0.1 mm × 0.2 mm × 0.5 mm in 2–3 weeks. The crystals were

cryoprotected by dipping in 100 μl drops of reservoir solution containing increasing concentrations of glycerol (first 5%, then 10%, then 20%), after which they were flash frozen in liquid nitrogen.

Data collection

A data set to 2.4 Å resolution was collected from two flash-frozen crystals at beamline A1 at the Cornell High Energy Synchrotron Source using a charge-coupled device detector (Area Detector Systems Corp., San Diego) and a wavelength of 0.914 Å. The crystals belonged to space group $P2_1$ with cell parameters a = 89.86 Å, b = 66.98 Å, c = 140.51 Å and β = 94.27°. For each of the two crystals, a low- and a high-resolution pass were recorded and processed independently with the programs DENZO and SCALEPACK [47]. The final data set, obtained after merging 240,859 observations of the individual data sets, contained 63,147 unique reflections (average redundancy = 3.8) and was 96% complete in the resolution range 20–2.4 Å (R_{Merge}(I) = 7.1%).

Structure determination and refinement

The structure of the VEGF–Fab complex was solved by molecular replacement. Taking into consideration the inherent twofold symmetry of the VEGF dimer, we expected that one VEGF dimer would be bound to two Fab molecules. Because of the absence of a crystallographic twofold rotation axis, the molecular dyad had to be noncrystallographic; thus the asymmetric unit would contain one VEGF dimer and two Fab fragments, yielding a Matthews parameter of 3.6 Å³/Da and a solvent content of 66%.

Rotation functions were calculated using a VEGF dimer as a search model ([12]; Brookhaven Protein Data Bank [PDB] accession code 2vpf). The crystal structure of a humanized anti-HER2 Fab fragment, anti-p185[HER2] ([27]; PDB accession code 1fvd), which had an 88% identical humanization framework [8,26], was used as a model for the Fab portion. In order to avoid bias, the CDRs were removed from the model and a tryptophan residue was substituted by alanine for additional verification purposes. A rotation search and Patterson correlation refinement [48] using the program XPLOR [49] yielded four distinct peaks for the VEGF dimer with correlation coefficients of 5.3–4.9%, while the subsequent highest peaks were below 4.3%. These four peaks correspond to two different candidate rotation solutions, pairs being related by the VEGF molecular dyad. Translation searches did not allow us to identify the correct solution.

With the Fab model, rotation searches calculated with data between 8 and 4 Å resolution, allowing the elbow angle [28] to vary between 110° and 210° in 10° steps yielded one (instead of two) unambiguous solution with a correlation coefficient of 9.8%, with the next peak at 5.6%. The pre-oriented Fab fragment could be readily translated into the unit cell with the program AMORE [50], and translation of the VEGF dimer with the Fab fragment fixed yielded an unambiguous solution for the highest of the two distinct VEGF rotation-solution candidates (R = 48.3% and correlation coefficient = 30.8%). Inspection of this solution with the program O [51] showed that the Fab CDRs would be in contact with VEGF, verifying the correctness of this partial solution, but the absence of any crystal packing contacts in one direction demonstrated that this model was still incomplete.

At this stage, refinement of the partial model was initiated. After rigid-body refinement followed by positional refinement with the program XPLOR [49] using all data between 10 and 3.0 Å resolution (R = 43.8%), clear electron density was observed for the omitted CDRs and tryptophan sidechain in a σ_A-weighted $(2F_o–F_c)exp(i\alpha_c)$ electron-density map [21]. After several rounds of positional refinement and manual rebuilding with the program O [51], all the CDRs of the Fab fragment could be built with confidence. Clear electron density emerged for the variable part of the second Fab molecule, related to the first Fab fragment via the molecular dyad of the VEGF dimer. After inclusion of this variable fragment, further positional refinement between 10 and 3.0 Å resolution yielded a crystallographic

R value of 31.9% (free R value = 38.0%) and maps into which the missing constant domain of the second Fab molecule was positioned, although clear density was only visible for those parts in immediate contact with the variable part of the molecule. Noncrystallographic symmetry restraints were applied in all further refinement, while gradually increasing the resolution to 2.4 Å, refining restrained individual temperature factors, and adding water molecules. At a late stage the structure factors were corrected for observed anisotropy, yielding the final model with a crystallographic R value of 19.6% (free R value = 26.6%) between 8 and 2.4 Å resolution. No bulk solvent correction was applied.

The final model is unusual with respect to the high average temperature factor of 100 Å² of the constant domain of the second Fab molecule. The use of noncrystallographic symmetry restraints forces this portion to be similar to the well-defined constant domain of the first Fab fragment. Therefore, although this domain contributes only weakly to the overall scattering and is thus poorly defined by the observed data, it could be accurately modeled because of the presence of the second identical and well-defined copy.

Construction of humanized anti-VEGF Fab phage

A monovalent, humanized Fab phagemid for alanine-scanning analysis was constructed by mutation of clone pMB16 (Figure 6), derived from phage humanization of the mAb A4.6.1 [7], to include additional substitutions identified in an optimally humanized variant of Fab-12 [8]. Mutations were made by site-directed mutagenesis [52], and verified by Sequenase (US Biochemical) sequencing. The new variant, pY0101 (Figure 6), contained the Fab-12 sequence, except for mutations Met4Leu in V_L and Thr231Leu in V_H. The former was retained from pMB16 in order to preclude possible methionine oxidation, and the latter was retained in order to retain the original junction (with amber codon for soluble Fab or Fab-g3p expression) sequence to the C-terminal domain of M13 g3p [7]. The Fab phagemid pY0101 was used for initial expression and affinity enhancement experiments in which the V_{L1} CDR residues 24 and 26–29 were randomized. Five codons in V_{L1} of pY0101 were first converted to stop (TAA) codons using the oligonucleotide 5′-GG GTC ACC ATC ACC TGC TAA GCA TAA TAA TAA TAA AGC AAC TAT TTA AAC TGG-3′. After verifying the stop-codon template by sequencing, a library was constructed by mutagenesis with a degenerate oligonucleotide (NNS replacing TAA codons). Fab-phage variants were propagated overnight in XL1-Blue *Escherichia coli* cells (Stratagene), then precipitated and sorted as described in [53]. VEGF binding selections yielded no affinity improvements compared with pY0101; however, one variant, pY0192 (Figure 6), was identified with a marked improvement in expression over pY0101. This clone, containing light chain mutations Ser24Arg, Ser26Asn, Gln27Glu, Asp28Gln, and Ile29Leu, as well as one heavy chain mutation Met34Ile, was used as the background for subsequent alanine-scanning mutagenesis. Each alanine substitution (or serine substitution for wild-type alanine) was constructed by site-directed mutagenesis and verified by DNA sequencing as described above.

VEGF binding assays using Fab-phage ELISA

Phage ELISA assays were performed and used to derive IC_{50} values as described [53]. Immunosorbant plates (Maxisorp plates, Nunc Intermed) were coated overnight at 4°C with 2 μg/ml VEGF in 50 mM carbonate buffer and blocked with 5% instant milk. For normalization of phage concentrations, serial dilutions of Fab phage were made in parallel in ELISA buffer (0.5% bovine serum albumin, 0.05% Tween-20 in phosphate-buffered saline (PBS) and incubated for 1 h at room temperature with immobilized VEGF. Plates were washed, incubated for 1 hour with rabbit anti-phage serum and horse radish peroxidase-conjugated goat anti-rabbit antibody (Pierce), washed again and developed with o-phenylenediamine substrate (Sigma). Normalized, subsaturating concentrations of phage for all Fab variants, as well as wild-type (pY0192), were mixed with serial dilutions (200 nM–0 nM) of VEGF in triplicate. The mixture was then added to VEGF-coated plates and analyzed as described above to determine an IC_{50} for each variant.

BIAcore analysis of Fab binding affinities

Y0192 Fab and several Fab variants were prepared by expression from the Fab-phagemid constructs by transforming the phagemids into a non-suppressor strain of *E. coli* [7]. Following induction of the PhoA pro-moter, cells were harvested and osmotically shocked, and the Fabs purified by protein G (Pharmacia) affinity chromatography [7]. Protein concentrations were determined using absorbance at 280 nm. Fab binding affinities were measured on a BIAcore-2000 (TM) system (BIAcore, Inc., Piscataway, NJ), essentially as previously described [7]. Carboxymethylated dextran biosensor chips (CM5, BIAcore Inc.) were activated with EDC (N-ethyl-N′-(3-dimethylaminopropyl)-carbodiimide hydrochloride) and NHS (N-hydroxysuccinimide) according to the suppli-er's instructions. VEGF in 20 mM sodium acetate, pH 4.8, was injected onto the biosensor chip at a concentration of 50 µg/ml to yield approxi-mately 700–1400 resonance-response units (RU) of covalently coupled protein. Unreacted groups were blocked with an injection of 1 M ethanolamine. Kinetics measurements were carried out by injecting twofold serial dilutions of Fab in running buffer (PBS containing 0.05% Tween-20) at 25°C using a flow rate of 20 µl/min. Association rates (k_{on}) and dissociation rates (k_{off}) were calculated using a simple one-to-one Langmuir binding model (BIAcore Evaluation Software v. 2.0; [54]). The equilibrium dissociation constant was calculated as the ratio k_{off}/k_{on}.

Alanine scan of the VEGF-interface residues

Fifty alanine mutants of VEGF had been previously generated and used to elaborate the KDR binding epitope on the hormone [15]. Nineteen of these mutant proteins (Table 3) were used to probe all the sidechain contacts with mAb A4.6.1 as observed in the crystal structure of the complex. For this study, each of these mutants was purified further by anion exchange (Pharmacia HiTrap Q, 1 ml), to remove traces of mis-folded monomer, which is known to interact with mAb A4.6.1. Binding affinities were measured with an ELISA that quantitated the binding of mAb A4.6.1 to immobilized VEGF in the presence of a dilution series of competing mutant [15].

Accession numbers

The coordinates and structure factors have been deposited with the Brookhaven Protein Data Bank for immediate release, with accession codes 1bj1 and 1bj1sf.

Acknowledgements

References

1. Dvorak, H.F., Brown, L.F., Detmar, M. & Dvorak, A.M. (1995). Vascular permeability factor/vascular endothelial growth factor, microvascular hyperpermeability and angiogenesis. *Am. J. Pathol.* **146**, 1029-1039.

2. Ferrara, N. (1995). The role of vascular endothelial growth factor in pathological angiogenesis. *Breast Cancer Res. Treat.* **36**, 127-137.

3. Folkman, J. (1995). Angiogenesis in cancer, vascular, rheumatoid and other disease. *Nat. Med.* **1**, 27-31.

4. Carmeliet, P., *et al.*, & Nagy, A. (1996). Abnormal blood vessel development and lethality in embryos lacking a single VEGF allele. *Nature* **380**, 435-439.

5. Ferrara, N., *et al.*, & Moore, M.W. (1996). Heterozygous embryonic lethality induced by targeted inactivation of the VEGF gene. *Nature* **380**, 439-442.

6. Kim, K.J., *et al.*, & Ferrara, N. (1993). Inhibition of vascular endothelial growth factor-induced angiogenesis suppresses tumour growth *in vivo*. *Nature* **362**, 841-844.

7. Baca, M., Presta, L.G., O'Connor, S.J. & Wells, J.A. (1997). Antibody humanization using monovalent phage display. *J. Biol. Chem.* **272**, 10678-10684.

8. Presta, L.G, *et al.*, & Ferrara, N. (1997). Humanization of an anti-vascular endothelial growth factor monoclonal antibody for the therapy of solid tumors and other disorders. *Cancer Res.* **47**, 4593-4599.

9. Waltenberger, J., Claesson-Welsh, L., Siegbahn, A., Shibuya, M. & Heldin, C.-H. (1994). Different signal transduction properties of KDR and Flt1, two receptors for vascular endothelial growth factor. *J. Biol. Chem.* **269**, 26988-26995.

10. Houck, K.A., Ferrara, N., Winer, J., Cachianes, G., Li, B. & Leung, D.W. (1991). The vascular endothelial growth factor family: identification of a fourth molecular species and characterization of alternative splicing of RNA. *Mol. Endocrinol.* **5**, 1806-1814.

11. Keyt, B.A., *et al.*, & Ferrara, N. (1996). The carboxyl-terminal domain (111-165) of vascular endothelial growth factor is critical for its mitogenic potency. *J. Biol. Chem.* **271**, 7788-7795.

12. Muller, Y.A., Christinger, H.W., Keyt, B.A. & De Vos, A.M. (1997). The crystal structure of vascular endothelial growth factor (VEGF) refined to 1.93 Å resolution: multiple copy flexibility and receptor binding. *Structure* **5**, 1325-1338.

13. Sun, P.D. & Davies, D.R. (1995). The cystine-knot growth-factor superfamily. *Annu. Rev. Biophys. Biomol. Struct.* **24**, 269-291.

14. Keyt, B.A., *et al.*, & Ferrara, N. (1996). Identification of vascular endothelial growth factor determinants for binding KDR and FLT-1 receptors. *J. Biol. Chem.* **271**, 5638-5646.

15. Muller, Y.A., Li, B., Christinger, H.W., Wells, J.A., Cunningham, B.C. & De Vos, A.M. (1997). Vascular endothelial growth factor: crystal structure and functional mapping of the kinase domain receptor binding site. *Proc. Natl Acad. Sci. USA* **94**, 7192-7197.

16. Wiesmann, C., Fuh, G., Christinger, H.W., Eigenbrot, C., Wells, J.A. & De Vos, A.M. (1997). Crystal structure at 1.7 Å resolution of VEGF in complex with domain 2 of the Flt-1 receptor. *Cell* **91**, 695-704.

17. Cunningham, B.C. & Wells, J.A. (1989). High-resolution epitope mapping of hGH-receptor interactions by alanine-scanning mutagenesis. *Science* **244**, 1081-1085.

18. Kelley, R.F. & O'Connell, M.P. (1993). Thermodynamic analysis of an antibody functional epitope. *Biochemistry* **32**, 6828-6835.

19. Wells, J.A. & De Vos, A.M. (1996). Hematopoietic receptor complexes. *Annu. Rev. Biochem.* **65**, 609-634.

20. Christinger, H.W., *et al.*, & De Vos, A.M. (1996). Crystallization of the receptor binding domain of vascular endothelial growth factor. *Proteins* **26,** 353-357.

21. Read, R.J. (1986). Improved Fourier coefficients for maps using partial structures with errors. *Acta Cryst. A* **42**, 140-149.

22. Laskowski, R.A., MacArthur, M.W., Moss, D.S. & Thornton, J.M. (1993). Procheck: a program to check the stereochemical quality of protein structures. *J. Appl. Cryst.* **26**, 283-291.

23. Sogabe, S., *et al.*, & Robinson, J.A. (1997). Neutralizing epitopes on the extracellular interferon γ receptor (IFNγR) α-chain characterized by homolog scanning mutagenesis and x-ray crystal structure of the A6 FAB-IFNγR$^{1-108}$ complex. *J. Mol. Biol.* **273**, 882-897.

24. Hoffman, D.W., Cameron, C.S., Davies, C., White, S.W. & Ramakrishnan, V. (1996). Ribosomal protein L9: a structure determination by the combined use of x-ray crystallography and NMR spectroscopy. *J. Mol. Biol.* **264**, 1058-1071.

25. Oefner, C., D'Arcy, A., Winkler, F.K., Eggimann, B. & Hosang, M. (1992). Crystal structure of human platelet-derived growth factor BB. *EMBO J.* **11**, 3921-3926.

26. Carter, P., *et al.*, & Shepard, H.M. (1992). Humanization of an anti-p185^{HER2} antibody for human cancer therapy. *Proc. Natl Acad. Sci. USA* **89**, 4285-4289.

27. Eigenbrot, C., Randal, M., Presta, L., Carter, P. & Kossiakoff, A.A. (1993). X-ray structures of the antigen-binding domains from three variants of humanized anti-p185^{HER2} antibody 4D5 and comparison with molecular modelling. *J. Mol. Biol.* **229**, 969-995.

28. Wilson, I.A. & Stanfield, R.L. (1994). Antibody-antigen interactions: new structures and new conformational changes. *Curr. Opin. Struct. Biol.* **4**, 857-867.

29. Chothia, C., *et al.*, & Poljak, R.J. (1989). Conformations of immunoglobulin hypervariable regions. *Nature* **342**, 877-883.

30. Bossart-Whitaker, P., Chang, C.Y.Y., Novotny, J., Benjamin, D.C. & Sheriff, S. (1995). The crystal structure of the antibody N10-Staphylococcal nuclease complex at 2.9 Å resolution. *J. Mol. Biol.* **253**, 559-575.

31. Chacko, S., *et al.*, & Sheriff, S. (1996). Refined structures of bobwhite quail lysozyme uncomplexed and complexed with the HyHEL-5 FAB fragment. *Proteins* **26**, 55-65.

32. Davies, D.R. & Cohen, G.H. (1996). Interactions of protein antigens with antibodies. *Proc. Natl Acad. Sci. USA* **93**, 7-12.
33. Jones, S. & Thornton, J.M. (1996). Principles of protein–protein interactions. *Proc. Natl Acad. Sci. USA* **93**, 13-20.
34. Wilson, I.A. & Stanfield, R.L. (1993). Antibody-antigen interactions. *Curr. Opin. Struct. Biol.* **3**, 113-118.
35. Wilmot, C.M. & Thornton, J.M. (1988). Analysis and prediction of the different types of β-turn in proteins. *J. Mol. Biol.* **203**, 221-232.
36. Padlan, E.A. (1990). On the nature of antibody combining sites: unusual structural features that may confer on these sites an enhanced capacity for binding ligands. *Proteins* **7**, 112-124.
37. Cunningham, B.C. & Wells, J.A. (1993). Comparison of a structural and a functional epitope. *J. Mol. Biol.* **234**, 554-563.
38. Novotny, J., Bruccoleri, R.E. & Saul, F.A. (1989). On the attribution of binding energy in antigen-antibody complexes McPC 603, D1-3, and HyHEL-5. *Biochemistry* **28**, 4735-4749.
39. Amit, A.G., Mariuzza, R.A., Phillips, S.E.V. & Poljak, R.J. (1986). Three-dimensional structure of an antigen-antibody complex at 2.8 Å resolution. *Science* **233**, 747-753.
40. Clackson, T., Ultsch, M.H., Wells, J.A. & De Vos, A.M. (1998). Structural and functional analysis of the 1:1 growth hormone:receptor complex reveals the molecular basis for receptor affinity. *J. Mol. Biol.* **277**, 1111-1128.
41. De Vos, A.M., Ultsch, M. & Kossiakoff, A.A. (1992). Human growth hormone and extracellular domain of its receptor: crystal structure of the complex. *Science* **225**, 306-312.
42. Clackson, T. & Wells, J.A. (1995). A hot spot of binding energy in a hormone-receptor interface. *Science* **267**, 383-386.
43. Banner, D.W., *et al.*, & Kirchhofer, D. (1996). The crystal structure of the complex of blood coagulation factor VIIa with soluble tissue factor. *Nature* **380**, 41-46.
44. Kelley, R.F., Costas, K.E., O'Connell, M.P. & Lazarus, R.A. (1995). Analysis of the factor VIIa binding site on human tissue factor: effects of tissue factor mutations on the kinetics and thermodynamics of binding. *Biochemistry* **34**, 10383-10392.
45. Mariuzza, R.A. & Poljak, R.J. (1993). The basics of binding: mechanisms of antigen recognition and mimicry by antibodies. *Curr. Opin. Immunol.* **5**, 50-55.
46. Webster, D.M., Henry, A.H. & Rees, A.R. (1994). Antibody-antigen interactions. *Curr. Opin. Struct. Biol.* **4**, 123-129.
47. Otwinowski, Z. (1993). Oscillation Data Reduction Program. In *Proceedings of the CCP4 Study Weekend: Data Collection and Processing.* (Sawyer, L., Isaacs, N. & Bailey, S. eds). pp. 56-62, SERC Daresbury Laboratory, UK.
48. Brünger, A.T. (1990). Extension of molecular replacement: a new search strategy based on Patterson correlation refinement. *Acta Cryst. A* **46**, 46-57.
49. Brünger, A.T., Kuriyan, J. & Karplus, M. (1987). Crystallographic R factor refinement by molecular dynamics. *Science* **235**, 458-460.
50. CCP4 (1994). The CCP4 suite: Programs for protein crystallography. *Acta Cryst. D* **50**, 760-763.
51. Jones, T.A., Zou, J.-Y., Cowan, S.W. & Kjeldgaard, M. (1991). Improved methods for building protein models in electron density maps and the location of errors in these models. *Acta Cryst. A* **47**, 110-119.
52. Kunkel, T.A., Bebenek, K. & McClary, J. (1991). Efficient site-directed mutagenesis using uracil-containing DNA. *Methods Enzymol.* **204**, 125-139.
53. Lowman, H.B. (1998). Phage display of peptide libraries on protein scaffolds. In *Methods in Molecular Biology*, *vol. 87: Combinatorial Peptide Library Protocols.* (Cabilly,S., ed.). pp. 249-264, Humana Press, Totowa, NJ, USA.
54. Karlsson, R., Michaelsson, A. & Mattson, A. (1991). Kinetic analysis of monoclonal antibody-antigen interactions with a new biosensor based analytical system *J. Immunol. Methods* **145**, 229-240.
55. Nicholls, A., Bharadwaj, R. & Honig, B. (1993). GRASP: graphical representation and analysis of surface properties. *Biophys. J.* **64**, 166-170.
56. Kabat, E.A., Wu, T.T., Redi-Miller, M., Perry, H.M. & Gottesman, K.S. (1987). *Sequences of Proteins of Immunological Interest, 4th Edition.* National Institute of Health, Bethesda, MD, USA.
57. Browner, M.F., Fauman, E.B. & Fletterick, R.J. (1992). Tracking conformational states in allosteric transitions of phosphorylase. *Biochemistry* **31**, 11297-11304.